Soft Matter

Cite this: *Soft Matter*, 2011, **7**, 5638

www.rsc.org/softmatter

PAPER

Multicompartment micelles from A_2-*star*-(B-*alt*-C) block terpolymers in selective solvents

Ching-I Huang,*[a] Cheng-Hsun Liao[a] and Timothy P. Lodge*[b]

Received 31st January 2011, Accepted 8th April 2011
DOI: 10.1039/c1sm05159h

The ability of multiblock ABC terpolymers to self-assemble into multicompartment micelles in an A-selective solvent is of great current interest. We have used dissipative particle dynamics (DPD) to explore the morphologies adopted by a particular block terpolymer architecture, A_2-*star*-(B-*alt*-C), where the two A blocks form the micelle corona and the alternating B and C blocks segregate within the core. Parameters of interest include the strength of the pairwise interactions among A, B, and C, the relative length of the A blocks compared to B + C, and the relative selectivity of the solvent towards B and C. A rich suite of structures are observed, including those with either spherical or wormlike cores, and with internally segregated B and C domains. Within the spherical micelle family, the B and C domains adopt various packings, including concentric layers, the "hamburger" motif (B–C–B layers and C–B–C layers), and a bicontinuous network. For wormlike micelles, the B and C domains are arranged as stacked alternating disks, or as intertwined helices. The choice of morphology is rationalized in terms of the relative block volume fractions and interaction energies. The DPD algorithm is a promising approach to screen ABC terpolymer architectures for the ability to produce potentially useful hierarchical structures.

1. Introduction

With advances in synthetic techniques, many copolymers with more complex molecular architectures or with more than two types of monomers have been successfully formulated. This development opens vast opportunities for a rich variety of more sophisticated morphologies with self-assembly on multiple length scales. The unique character of such hierarchical structures offers new material properties and thus novel technologies and applications.[1–4] Recently, interest has grown in a class of copolymers containing one or two long end-blocks and multiple short mid-blocks.[5–16]

It has been shown that they can form a series of hierarchical structure-within-structure morphologies. For example, Matsushita *et al.* synthesized an undecablock terpolymer consisting of two long poly(2-vinylpyridine) end-blocks and short polystyrene–polyisoprene alternating middle-blocks, and observed the formation of spheres-within-lamellae, cylinders-within-lamellae, lamellae-within-lamellae, coaxial cylinders, and concentric spheres.[7] This series of hierarchical structures as a function of composition has also been reported theoretically in our recent work by employing dissipative particle dynamics (DPD) to simulate the self-assembling behavior.[13] In particular, we chose A_2-*star*-(B-*alt*-C) molecules, in which multiple short B and C alternating blocks are linked to the middle of a long A-block, instead of the end of A-block (referred as A-*block*-(B-*alt*-C)), as shown in Fig. 1. This architectural choice is motivated by the fact that the simulation box and time can be reduced. Despite this difference of molecular architecture between the simulated A_2-*star*-(B-*alt*-C) and experimental A-*block*-(B-*alt*-C) or A-*block*-(B-*alt*-C)-*block*-A, they are expected to exhibit similar phase behavior. Indeed, both AB linear and A_2B star copolymers also exhibit similar morphology patterns.[17,18] Recently, Zhang *et al.* employed the real-space self-consistent mean-field theory to investigate the self-assembled microstructures formed by A-*block*-(B-*alt*-C) copolymers.[16] They obtained similar types of parallel packed hierarchical structure-within-structures for most

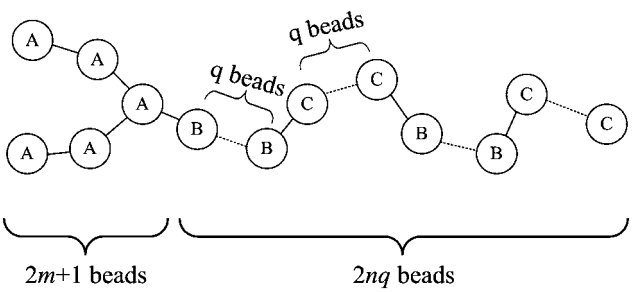

Fig. 1 A schematic plot of the model A_2-*star*-(B-*alt*-C) molecules.

[a]*Institute of Polymer Science and Engineering, National Taiwan University, Taipei, 106, Taiwan. E-mail: chingih@ntu.edu.tw*
[b]*Department of Chemistry and Department of Chemical Engineering and Materials Science, University of Minnesota, Minneapolis, Minnesota, 55455-0431, USA. E-mail: lodge@umn.edu*

interaction parameters between components i and j, χ_{ij}; one exception is when $\chi_{BC} \gg \chi_{AB} > \chi_{AC}$, the multiblock copolymers form B and C segregated small-length-scale domains perpendicular to the large-length scale domains. Later, we will show that these perpendicular packed hierarchical microstructures can be more easily tailored in solution by varying the solvent selectivity.

In addition to hierarchical structures in bulk, ABC multiblock terpolymers have been shown to be excellent candidates for forming multicompartment micelles, in which the two solvophobic blocks (B and C) adopt distinct nanodomains within the micellar cores, while the solvophilic A chains provide the stabilizing corona.[19–22] Multicompartment micelles, within which the multiple segregated domains are able to store and deliver two or more agents simultaneously, have been targeted potentially for advanced applications in drug delivery and gene therapy.[3,4] Linear ABC terpolymers tend to form core–shell–corona micelles,[23–31] but ABC mikto-arm star terpolymers exhibit a much richer array of structures, due to the architectural constraint that the A, B, and C domains meet at common curves in space.[21,32–41] Clearly, the parameter space for designing terpolymers to adopt interesting hierarchical structures is huge, and thus there is a need for theoretical approaches capable of exploring "morphology maps" as a function of the molecular variables.

As demonstrated experimentally and theoretically, A-coil/BC-alternating multiblock terpolymers exhibit the ability to form hierarchical structures. In particular, when the fraction of the BC-blocks is low, they tend to form multiple B and C coaxial cylinders or concentric spheres in a matrix of the majority A component. Moreover, the number of small-length-scale B and C layers increases with the number of alternating B and C short blocks.[6,13,15] In this paper we explore the self-assembling behavior of coil-alternating multiblock terpolymers into multicompartment micelles in the presence of a selective solvent for A. As a starting point, we choose the previously simulated architecture of A_2-*star*-(B-*alt*-C). We employ the dissipative particle dynamics (DPD) technique[42,43] as it has enabled us to reproduce the various types of hierarchical structures formed experimentally by similar multiblock copolymers.[13] Generally, the DPD method simplifies a long series of molecular groups into a few bead-and-spring type particles, and therefore it can access molecular behavior on longer time-scales and larger length-scales compared with classical molecular dynamics and Monte Carlo simulations. In particular, we focus on the effects of solvent selectivity and copolymer composition. To our knowledge, the effects of solvent addition on the resultant phase behavior of A_2-*star*-(B-*alt*-C) molecules have not been addressed yet, either experimentally or theoretically.

2. DPD simulation method and model parameters

In the DPD simulation,[42] the time evolution of motion for a set of interacting particles is solved by Newton's equation. For simplicity, we assume that the masses of all particles are equal to 1. The force acting on the i-th particle $\vec{f}_i$ contains three parts: a conservative force $\vec{F}_{ij}^{C}$, a dissipative force $\vec{F}_{ij}^{D}$, and a random force $\vec{F}_{ij}^{R}$, *i.e.*,

$$\vec{f}_i = \sum_{i \neq j} \left(\vec{F}_{ij}^{C} + \vec{F}_{ij}^{D} + \vec{F}_{ij}^{R} \right) \quad (1)$$

where the sum is over all other particles within a certain cut-off radius r_c. As this short-range cut-off counts only local interactions, r_c is usually set to 1 so that all lengths are measured relative to the particle radius.

The conservative force $\vec{F}_{ij}^{C}$ is a soft repulsive force given by

$$\vec{F}_{ij}^{C} = \begin{cases} -a_{ij}\left(1 - \dfrac{r_{ij}}{r_c}\right)\vec{n}_{ij} & r_{ij} < r_c \\ 0 & r_{ij} \geq r_c \end{cases} \quad (2)$$

where a_{ij} is the repulsive interaction parameter between particles i and j, $\vec{r}_{ij} = \vec{r}_j - \vec{r}_i$, $r_{ij} = |\vec{r}_{ij}|$, and $\vec{n}_{ij} = \dfrac{\vec{r}_{ij}}{r_{ij}}$.

The dissipative force $\vec{F}_{ij}^{D}$ is a hydrodynamic drag force given by

$$\vec{F}_{ij}^{D} = \begin{cases} -\gamma \omega^{D}(r_{ij})(\vec{n}_{ij}\,\vec{v}_{ij})\vec{n}_{ij} & r_{ij} < r_c \\ 0 & r_{ij} \geq r_c \end{cases} \quad (3)$$

where γ is a friction coefficient, ω^{D} is an r-dependent weight function vanishing for $r \geq r_c$, and $\vec{v}_{ij} = \vec{v}_j - \vec{v}_i$

The random force $\vec{F}_{ij}^{R}$ corresponds to the thermal noise and has the form

$$\vec{F}_{ij}^{R} = \begin{cases} \sigma \omega^{R}(r_{ij})\theta_{ij}\vec{n}_{ij} & r_{ij} < r_c \\ 0 & r_{ij} \geq r_c \end{cases} \quad (4)$$

where σ is a parameter, ω^{R} is a weight function, and $\theta_{ij}(t)$ is a randomly fluctuating variable. Note that these two forces $\vec{F}_{ij}^{D}$ and $\vec{F}_{ij}^{R}$ also act along the line of centers and conserve linear and angular momentum. There is an independent random function for each pair of particles. Also there is a relation between both constants γ and σ as follows,[43]

$$\sigma^2 = 2\gamma k_B T \quad (5)$$

In our simulations, $\gamma = 4.5$ and the temperature $k_B T = 1$. As such, $\sigma = 3.0$ according to eqn (5).

In order for the steady-state solution to the equation of motion to be the Gibbs ensemble and for the fluctuation–dissipation theorem to be satisfied, it has been shown that only one of the two weight functions ω^{D} and ω^{R} can be chosen arbitrarily,[44]

$$\omega^{D}(r) = [\omega^{R}(r)]^2 \quad (6)$$

and is usually taken as

$$\omega^{D}(r) = \left[\omega^{R}(r)\right]^2 = \begin{cases} \left(1 - \dfrac{r_{ij}}{r_c}\right)^2 & r_{ij} < r_c \\ 0 & r_{ij} \geq r_c \end{cases} \quad (7)$$

Finally, the spring force $\vec{f}^{S}$, which acts between the connected beads in a molecule, has the form of

$$\vec{f}_i^{S} = \sum_j C\vec{r}_{ij} \quad (8)$$

where C is a harmonic type spring constant for the connecting pairs of beads in a molecule, and is set equal to 4 (in units of $k_B T$).[43]

Note that a modified version of the velocity-Verlet algorithm is used here to solve the Newtonian equation of motion[45]

$$\begin{aligned} r_i(t+\Delta t) &= r_i(t) + v_i(t)\Delta t + \frac{1}{2} f_i(t)\Delta t^2 \\ \tilde{v}_i(t+\Delta t) &= v_i(t) + \lambda f_i(t)\Delta t \\ f_i(t+\Delta t) &= f_i[r_i(t+\Delta t), \tilde{v}_i(t+\Delta t)] \\ v_i(t+\Delta t) &= v_i(t) + \frac{1}{2}\Delta t[f_i(t) + f_i(t+\Delta t)] \end{aligned} \quad (9)$$

The parameter λ is introduced to account for some additional effects of the stochastic interactions. A detailed investigation of the effects of λ on the steady state temperature has been reported by Groot and Warren.[43] For particle density $\rho = 3$ and the constant $\sigma = 3$, they found an optimum value of $\lambda = 0.65$, in which the temperature control can be significantly maintained even at a large time step of 0.06. Here, we choose $\lambda = 0.65$ and the time step $\Delta t = 0.05$ according to ref. 43. It should be mentioned that a few studies pointed out this choice of $\Delta t = 0.05$ still enables the systems to artificially experience a significant degree of thermal fluctuation.[46,47] Thus, the simulated patterns may reflect the effects associated with not only the thermodynamic parameters but also some degree of artificially numerical errors. However, as the time-step is chosen the same throughout the systems examined here, the induced artificial effects should be the same. Accordingly, our simulated phase maps of micelle morphology can still be rationalized qualitatively as a function of the thermodynamically equilibrium parameters.

The DPD simulations are performed in a cubic box of L^3 grids with periodic boundary conditions. The particle density ρ is set equal to 3. Hence, the total number of simulated DPD beads is $3L^3$. On the basis of the algorithm described above, the time evolution of motion for these particles starts with an initially disordered configuration and is simulated within a cubic box. Each simulation is performed until the structure remains unchanged with subsequent time steps. In general, the resultant morphology patterns *via* DPD depend on the finite size of the simulation box, as has been reported in other studies.[48–50] In order to exclude the finite size effects, we were careful to enlarge the simulation box size until the structures were no longer affected by the simulation box. For our current model systems examined here, a simulated box size of 30 × 30 × 30 was chosen. Each simulation was performed about 500 000–600 000 steps, which takes about 48 h of CPU time of Pentium D820.

The model A_2-*star*-(B-*alt*-C) chain, as displayed in Fig. 1, consists of n alternating B–C blocks, grafted onto the middle of the coil A block with $2m + 1$ beads. Each B and C alternating block is represented by q beads. The total number of beads per chain N is thus equal to $(2m + 1) + 2nq$. Here, we use two beads to represent each alternating B and C block (*i.e.* $q = 2$) to allow more conformational freedom of each alternating B and C block. In simulating the multicompartment micelles formed by the A_2-*star*-(B-*alt*-C) molecules in a selective solvent S, we set the total number of beads per chain N and the copolymer volume fraction ϕ equal to 33 and 0.13, respectively. The copolymer consists of a solvophilic A block ($a_{AS} = 25$) and solvophobic B and C blocks (a_{BS} and $a_{CS} > 25$). Since the interaction parameters between the A-block and the BC-alternating block, that is, a_{AB} and a_{AC}, play a dominant role in the large length-scale diblock-like segregation, we assume $a_{AB} = a_{AC}$ to reduce one interaction variable. Accordingly, the formation of multicompartment micelles is explored by varying the A composition f_A, which is equal to $(2m + 1)/N$, and the interaction parameters of $a_{AB} = a_{AC}$, a_{BC}, a_{BS}, and a_{CS}.

The dimensionless interaction parameter (*i.e.*, in terms of k_BT) between like particles was set at $a_{ii} = 25$ for the particle density $\rho = 3$, following of Groot and Warren.[43] The interaction parameter between different components i and j can be estimated by the following relationship between a_{ij} and the Flory–Huggins interaction parameter χ_{ij} derived by Groot and Warren[43] for $\rho = 3$,

$$a_{ij}(T) = a_{ii} + 3.497\chi_{ij}(T);\ i,j = \text{A, B, and C} \quad (10)$$

Therefore, any value of $a_{ij} \leq 25$ corresponds to $\chi_{ij} \leq 0$, which indicates that components i and j are very miscible. As the incompatibility between i and j increases, a_{ij} increases from 25. It should be noted that as the simulated chains *via* DPD are short, one has to consider the fluctuation effects associated with a finite chain in order to map out the relationship between the effective χ_{ij} and a_{ij}. For example, when simulating the phase behavior of linear AB diblock copolymers *via* DPD, Groot *et al.* have quantitatively matched the phase diagrams between the DPD simulation and SCMF theory by applying the following equation,[51]

$$(\chi_{AB}N)_{eff} = \frac{\chi_{AB}N}{1 + 3.9N^{-0.51}} \quad (11)$$

which was first derived by Fredrickson and Helfand.[52] Though our simulated molecular architecture is different, it is still a good starting point to estimate the effective χN value for a given a. In our work, when considering the large-length-scale segregation between the solvophilic A and the solvophobic B and C, a typical value of interaction parameter, $a_{AB} = a_{AC} = 50$, for a copolymer chain $N = 33$, corresponds to $(\chi N)_{eff} = 142$, indicating a very strong segregation of the copolymer itself. When considering the small-length-scale segregation between B and C, we set each B and C block has only 2 beads and thus $N = N_B + N_C = 4$. The value of $a_{BC} = 30$–120 corresponds to $(\chi N)_{eff} = 2$–37. Later in the

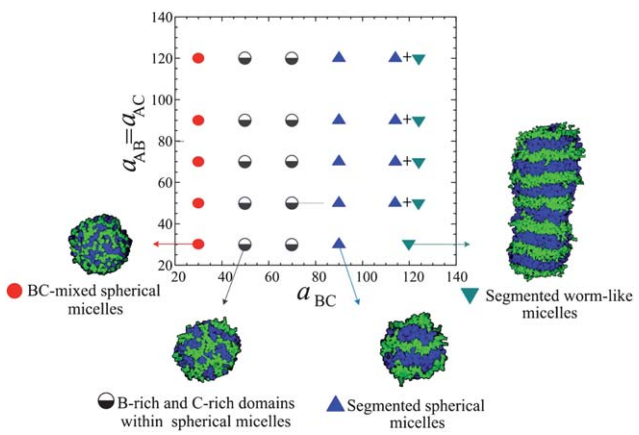

Fig. 2 Phase diagram of A_2-*star*-(B-*alt*-C) copolymer with $f_A = 0.27$ and $N = 33$ in a selective solvent with $a_{AS} = 25$, $a_{BS} = a_{CS} = 50$, and $\phi = 0.13$ in terms of the interaction parameters $a_{AB} = a_{AC}$ and a_{BC}. The same symbols represent similar micellar structures. In each representative micelle, B and C domains are shown *via* the green and blue colors, respectively, and both components of solvophilic A and solvent S are omitted, for clarity.

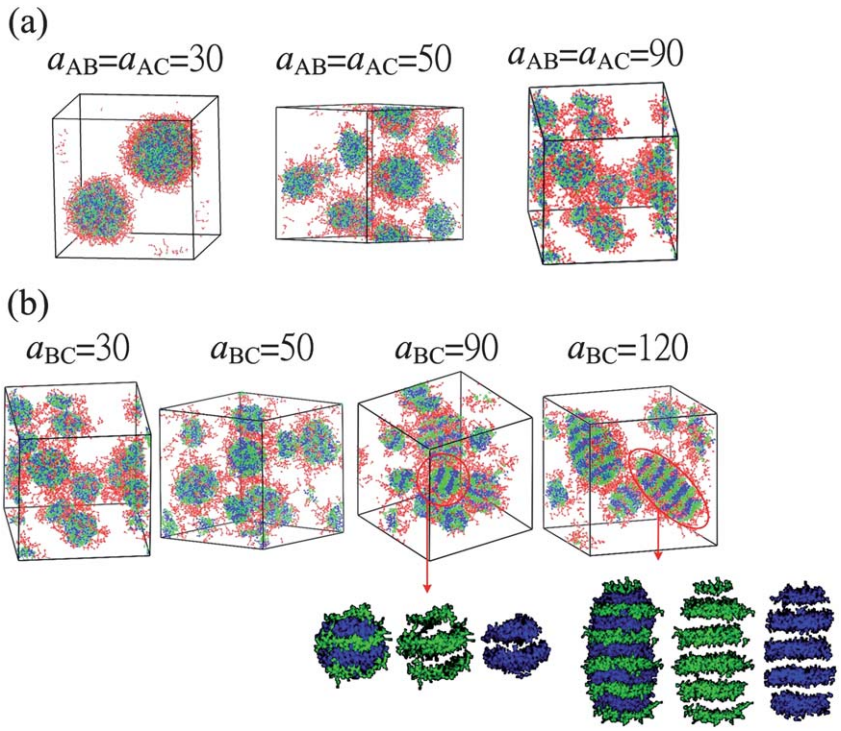

Fig. 3 Morphological variation of A_2-*star*-(B-*alt*-C) copolymer solutions when $f_A = 0.27$, $N = 33$, $a_{AS} = 25$, $a_{BS} = a_{CS} = 50$, and $\phi = 0.13$, with (a) $a_{AB} = a_{AC}$ when $a_{BC} = 30$, and (b) a_{BC} when $a_{AB} = a_{AC} = 90$. The red, green, and blue colors represent A, B, and C, respectively. Solvent S is omitted here for clarity.

Results and discussion, it is reasonable to observe a series of transition from a miscible state of B and C ($a_{BC} = 30$, *i.e.*, $(\chi N)_{eff} = 2$) to partially segregated B-rich and C-rich domains ($a_{BC} = 50$–70, *i.e.*, $(\chi N)_{eff} = 10$–17) and then to well segregated B and C layers ($a_{BC} \geqq 90$, *i.e.*, $(\chi N)_{eff} \geqq 25$).

3. Results and discussion

In this section, we first discuss the situation where the solvent S is neutral to both solvophobic blocks B and C ($a_{BS} = a_{CS}$), and then extend to the more general case with differing degrees of solvent phobicity ($a_{BS} \neq a_{CS}$).

Symmetric interaction parameters of $a_{BS} = a_{CS}$

We first choose $f_A = 0.27$, $N = 33$ (the number of alternating B–C blocks, $n = 6$) $\phi = 0.13$, $a_{AS} = 25$, $a_{BS} = a_{CS} = 50$, and construct the corresponding morphology map in terms of $a_{AB} = a_{AC}$ and a_{BC} in Fig. 2. At a fixed value of a_{BC}, we observe that varying $a_{AB} = a_{AC}$ has little effect on the structure of the formed micelles. A typical morphology variation with $a_{AB} = a_{AC}$ is illustrated in Fig. 3a, for a_{BC} is fixed at 30. In this case, even when $a_{AB} = a_{AC}$ decreases to a low value of 30, the formed micelles are still BC-miscible spheres. However, with decreasing incompatibility between solvophilic A and solvophobic B and C components, these solvophilic A blocks tend to mix with BC-alternating blocks. Thus, larger spherical micelles can be formed as $a_{AB} = a_{AC}$ decreases. When a_{BC} increases one expects a more obvious small-length-scale segregation between B and C blocks within the spheres, as shown in Fig. 3b where we display the micellar patterns at $a_{AB} = a_{AC} = 90$. Moreover, when a_{BC} increases to a large value of 120, a larger-length-scale transition from B and C segmented spheres to worm-like micelles is observed. This is also not surprising since when a_{BC} increases, the BC-alternating

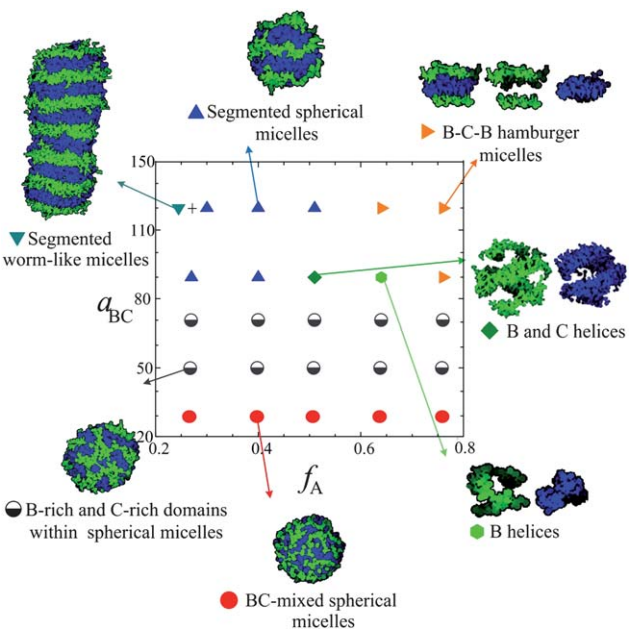

Fig. 4 Phase diagram of A_2-*star*-(B-*alt*-C) copolymer solutions in terms of the interaction parameter a_{BC} and the A composition f_A when $N = 33$, $a_{AB} = a_{AC} = 50$, $a_{AS} = 25$, $a_{BS} = a_{CS} = 50$, and $\phi = 0.13$. The same symbols represent similar micellar structures. In each representative micelle, B and C domains are shown *via* the green and blue colors, respectively, and both A and S are omitted, for clarity.

chains would rather stretch more to form more B and C segregated layers with micelles in order to reduce the contacts between B and C.

As demonstrated above, varying the incompatibility degree between B and C, a_{BC}, not only affects the formation of small-length-scale segregation between B and C but also the large-length-scale micelle geometry, whereas varying $a_{AB} = a_{AC}$ does not. Similarly, varying the number of B and C alternating blocks or composition f_A also has a great influence on the topology of the overall shape of micelles. In order to illustrate this effect associated with f_A or n, we fix the value of $N = 33$, $a_{AS} = 25$, $a_{BS} = a_{CS} = 50$, $a_{AB} = a_{AC} = 50$, and construct the corresponding phase diagram in terms of f_A and a_{BC}, as shown in Fig. 4. In addition, Fig. 5a–c displays some of the simulated morphologies as a function of f_A when $a_{BC} = 70$, 120, and 90, respectively. When a_{BC} is not large enough to ensure that the two solvophobic blocks of B and C are well segregated, only spherical micelles are observed in this wide range of $f_A = 0.27$–0.76 (n varies from 6 to 2), as displayed in Fig. 5a for $a_{BC} = 70$. Once a_{BC} increases significantly ($a_{BC} > 70$), the fact that B and C are well segregated within micelles enables the formation of various micelle patterns induced by varying the composition f_A. For example, when

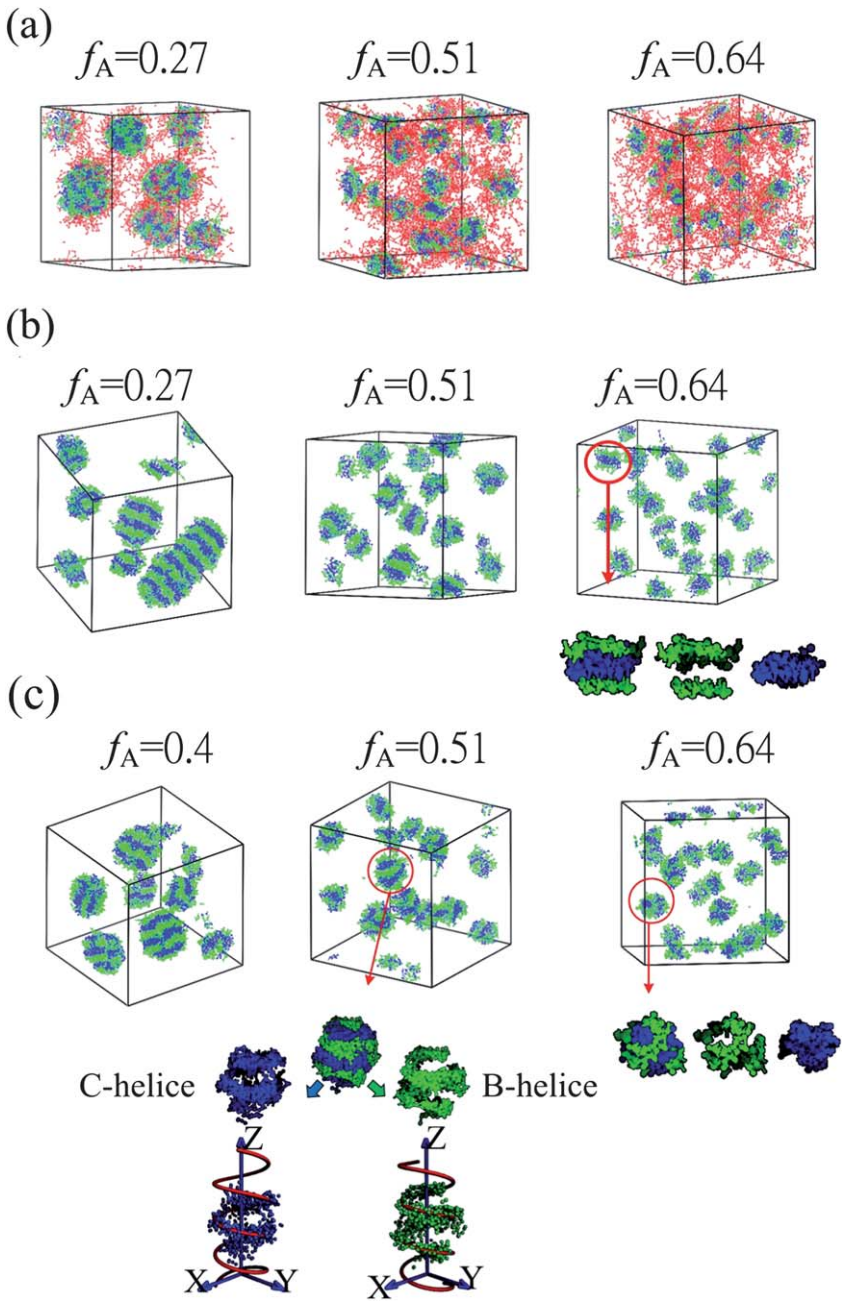

Fig. 5 Simulated morphology patterns as a function of f_A when a_{BC} = (a) 70, (b) 120, and (c) 90, respectively. All the other parameters are the same as those in Fig. 4. The red, green, and blue colors represent A, B, and C, respectively. Solvent S is omitted here for clarity. In (c), both B and C domains are fitted very well by the helical curves, which are shown as the solid lines, with pitch and radius equal to 3.8 and 3.0 (grid size), respectively.

$a_{BC} = 120$ (Fig. 5b), a series of transitions from BC-segmented worm-like micelles ($f_A = 0.27$, $n = 6$) → BC-segmented spherical micelles ($f_A = 0.3$–0.5, $n = 5$–4) → B–C–B hamburger micelles ($f_A = 0.6$–0.8, $n = 3$–2) occurs with an increase in f_A. This is reasonable since the number of BC-alternating blocks decreases with increasing f_A, and the number of the B and C segregated layers formed within micellar domains decreases, and thus we observe a variation of the micelle type from worm-like → spherical → hamburger micelles. However, it is interesting to note that when a_{BC} decreases to 90, as shown in Fig. 5c, in addition to the BC-segmented spherical micelles ($f_A = 0.2$–0.4) and B–C–B hamburger micelles ($f_A = 0.7$–0.8), these molecules tend to form B and C helices or a single B helix when f_A is in the intermediate region of 0.5–0.6. The fact that A_2-*star*-(B-*alt*-C) molecules can form helical structures when both $f_A(n)$ and a_{BC} are in the intermediate region can be interpreted as follows. Recall that a_{BC} has to be large enough to ensure good segregation between B and C; but too large a value of a_{BC} enables them to form a packing of discrete B and C segregated layers within micelles. It is thus possible for the B and C segregated domains to connect, respectively, and form continuous structures at intermediate values of a_{BC}. However, with a decrease in f_A (an increase in n), based on the fact that more B and C alternating blocks segregate into one micelle, it is easier to form discrete segmented domains as long as a_{BC} exceeds the threshold value for B and C segregation. This can also be seen in Fig. 4: when f_A is in the region of 0.2–0.4, a series of transitions from BC-mixed spheres → B and C partially segregated spheres → segmented spherical and worm-like micelles occurs with increasing a_{BC}. In contrast, if f_A increases to a large value, for example 0.75, the segregated B and C domains are not large enough to connect and form continuous helices; thus we only observe the formation of

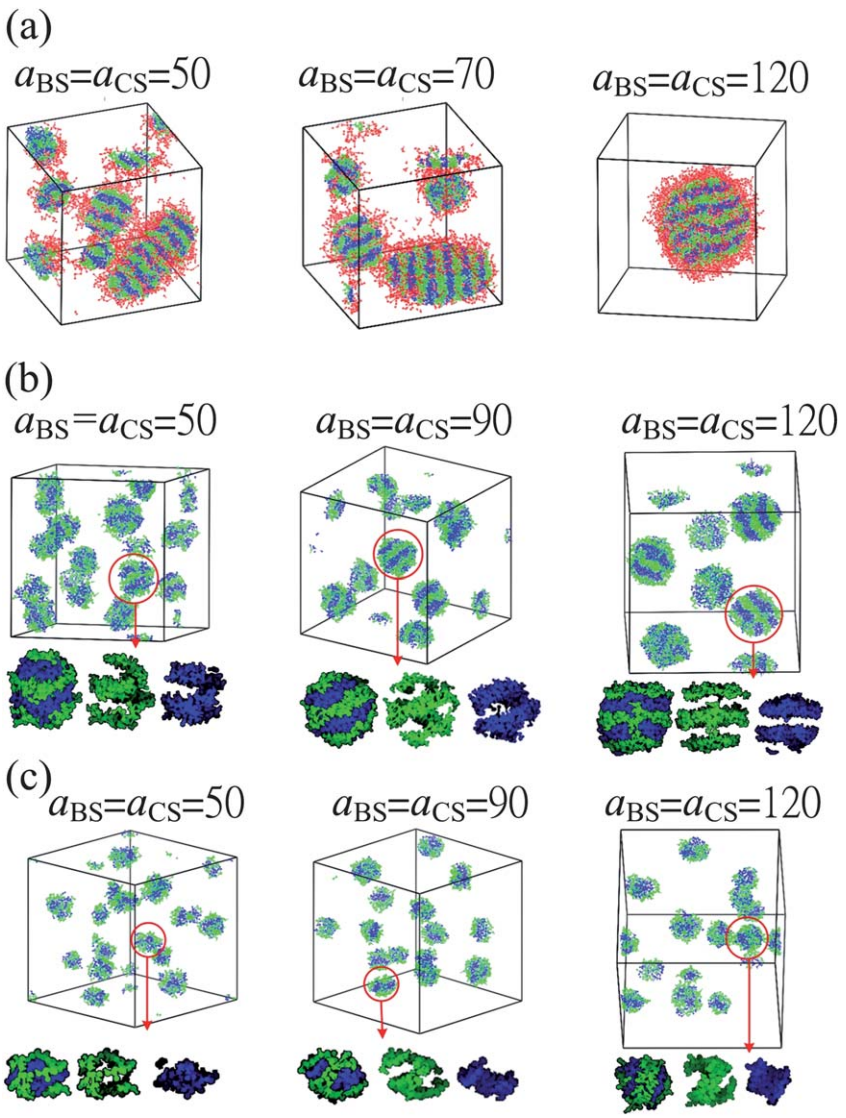

Fig. 6 Morphological patterns as a function of $a_{BS} = a_{CS}$ when (a) $f_A = 0.27$, $a_{BC} = 120$, (b) $f_A = 0.51$, $a_{BC} = 90$, and (c) $f_A = 0.7$, $a_{BC} = 90$, respectively. All the other parameters are set as $N = 33$, $a_{AB} = a_{AC} = 50$, $a_{AS} = 25$, $\phi = 0.13$. The red, green, and blue colors represent A, B, and C, respectively. Solvent S is omitted here for clarity.

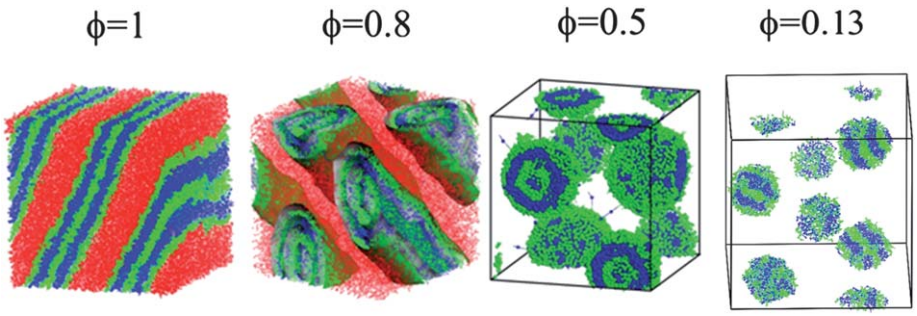

Fig. 7 Morphological variation of A_2-*star*-(B-*alt*-C) copolymer solutions with ϕ when $f_A = 0.51$, $N = 33$, $a_{AB} = a_{AC} = 50$, $a_{BC} = 120$, $a_{AS} = 25$, and $a_{BS} = a_{CS} = 100$. The red, green, and blue colors represent A, B, and C, respectively. Solvent S is omitted here for clarity.

B–C–B hamburgers when a_{BC} exceeds the segregation threshold value. This adoption of a helical morphology is reminiscent of the behavior of diblock copolymers confined in nanoscopic cylindrical channels.[53]

Finally, in the neutral case with $a_{BS} = a_{CS}$, we would like to explore how the resultant micelle morphology is affected by the degree of solvophobicity. For this purpose, we choose three specific micelle types: segmented worm-like or spherical micelles, B and C helices, and a single B helix, which are formed when $f_A = 0.27$ and $a_{BC} = 120$, $f_A = 0.51$ and $a_{BC} = 90$, and $f_A = 0.7$and $a_{BC} = 90$, respectively. We fix $N = 33$ ($n = 6$) $a_{AB} = a_{AC} = 50$, $a_{AS} = 25$, $a_{BS} = a_{CS} = 50$, and then increase the value of $a_{BS} = a_{CS}$ to 120. Fig. 6a–c displays the corresponding patterns, respectively, as a function of $a_{BS} = a_{CS}$. As expected, in order to avoid the contacts between solvent and B or C with an increasing degree of solvophobicity of B and C, more chains are forced into one micelle, within which the segregated B-rich and C-rich layers grow in the radial direction. Therefore, it is clear to observe the formation of larger and more spherical B and C segmented micelles with an increase in $a_{BS} = a_{CS}$ to 120 for the copolymer with $f_A = 0.27$ in Fig. 6a. For the copolymers with $f_A = 0.51$ and $f_A = 0.7$, which tend to form continuous helical structures, we observe that increasing $a_{BS} = a_{CS}$ can also enhance the effective segregation between B and C into the formation of discrete B and C alternating layers. Thus we observe a transition from B and C helices to segmented spherical micelles (Fig. 6b), and a B helix to B–C–B hamburgers (Fig. 6c), by increasing $a_{BS} = a_{CS}$ from 50 to 120 for $f_A = 0.51$ and 0.7, respectively.

The above results demonstrated the significant effects associated with the composition (f_A), the interaction between the two solvophobic blocks (a_{BC}), and interfacial tension (a_{BS} and a_{CS}), on the shape and internal packing of multicompartment micelles when the solvent is neutral to both B and C ($a_{BS} = a_{CS}$). Next, we address the difference of the packing of the small-length-scale B and C segregated layers generated in the melt and solution. Fig. 7 illustrates the simulated morphology patterns as a function of copolymer volume fraction ϕ when $f_A = 0.51$, $N = 33$, $a_{AB} = a_{AC} = 50$, $a_{BC} = 120$, $a_{BS} = a_{CS} = 100$, and $a_{AS} = 25$. As ϕ decreases, a series of large-length-scale morphology transitions from lamellae → BC-cylinders → BC-spheres is observed. This trend is analogous to decreasing the combined fraction of B and C blocks in the melt, since the solvent S prefers the A block to the B and C components. Further, we observe that with decreasing ϕ from 1.0 to 0.5, the B and C alternating layers pack in a parallel direction to the large-length-scale lamellae, or in a coaxial and concentric direction to cylinders and spheres, respectively. But when ϕ decreases to less than 0.2, the formed micelles become B and C segmented spheres. Generally, the formation of micelles in less concentrated solution is mainly driven by the solvophobicity of the B and C blocks. Accordingly, when a_{BC} is large enough to assure good segregation between B and C blocks within micelles, the formed B and C segregated lamellae tend to pack in a perpendicular direction with respect to the BC-rich and S-rich domains, in order to have equal interfacial area with S. Whereas, in the melt, despite the equal degree of incompatibility between A/C and A/B, the constraint of molecular architecture that the A coil blocks are connected with a B-block first imposes more contacts between A and B. Thus, the formed B and C small-length-scale domains with respect to the large-length-scale lamellae, cylinders, and spheres are typically parallel, coaxial, and concentric, respectively, in melts and/or concentrated solutions.[13]

Asymmetric interaction parameters with respect to the solvent $a_{BS} \neq a_{CS}$

Here we relax the previous restriction of $a_{BS} = a_{CS}$ to investigate the effects of solvent selectivity with respect to the B and C blocks. To reach this goal, we again choose the three

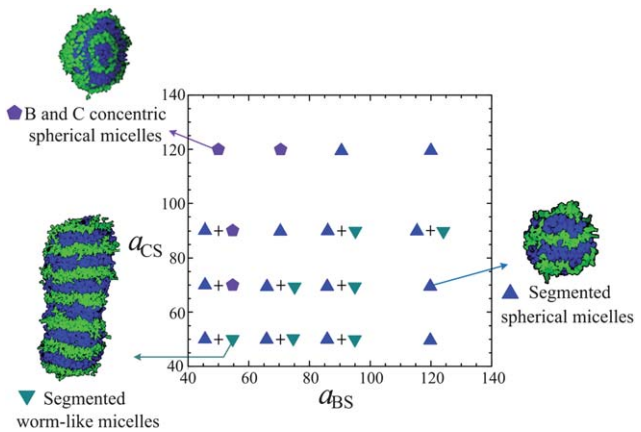

Fig. 8 Phase diagram of A_2-*star*-(B-*alt*-C) copolymer solutions in terms of a_{BS} and a_{CS} when $f_A = 0.27$, $N = 33$, $\phi = 0.13$, $a_{AB} = a_{AC} = 50$, $a_{BC} = 120$, and $a_{AS} = 25$. The same symbols represent similar micellar structures. In each representative micelle, B and C domains are shown *via* the green and blue colors, respectively, and both A and S are omitted, for clarity.

representative micelle types frequently formed when $a_{BS} = a_{CS}$: worm-like and spherical micelles, B and C helices, and a single B helix, as shown in Fig. 6a–c, respectively. We examine how these three types of micelles are affected by varying the relative values of a_{BS} and a_{CS}.

In Fig. 8 we present the corresponding morphology map in terms of a_{BS} and a_{CS} for the first case when f_A is small (for example, 0.27). When $a_{CS} > a_{BS}$, the larger solvophobicity of C enables the B component to be pulled closer to the outside S solvent and A component. Thus, a concentric packing of the B and C segregated layers within micelles is more favored than the segmented packing when the C blocks become more solvophobic than B. We can find a more stable region of the multiple BC-segregated concentric spheres when a_{CS} is significantly larger than a_{BS} in Fig. 8. A typical morphology variation with a_{CS} at a fixed value of $a_{BS} = 50$ is shown in Fig. 9a. A gradual transition from the B and C segmented worm-like and spherical micelles into the concentric BC-segregated spheres is clear as a_{CS} increases from 50 to 120. In contrast, when $a_{BS} > a_{CS}$, one may expect that the C component would be pulled closer to the S (A) components and thus the formation of concentric spheres but with C in the outermost shell. However, as designated in Fig. 8, the formed micelle types are still B and C segmented worm-like and spherical micelles, but within which the top and bottom layers are formed by C instead of B. The formation of segmented micelles instead of concentric micelles is mainly attributable to the molecular architecture in that the A-coil is connected with B, which makes it difficult to keep B completely away from A (S) by forming a perfect outermost C-shell. A further examination of the micelle formation with time at $a_{BS} = 90$ and 120 is

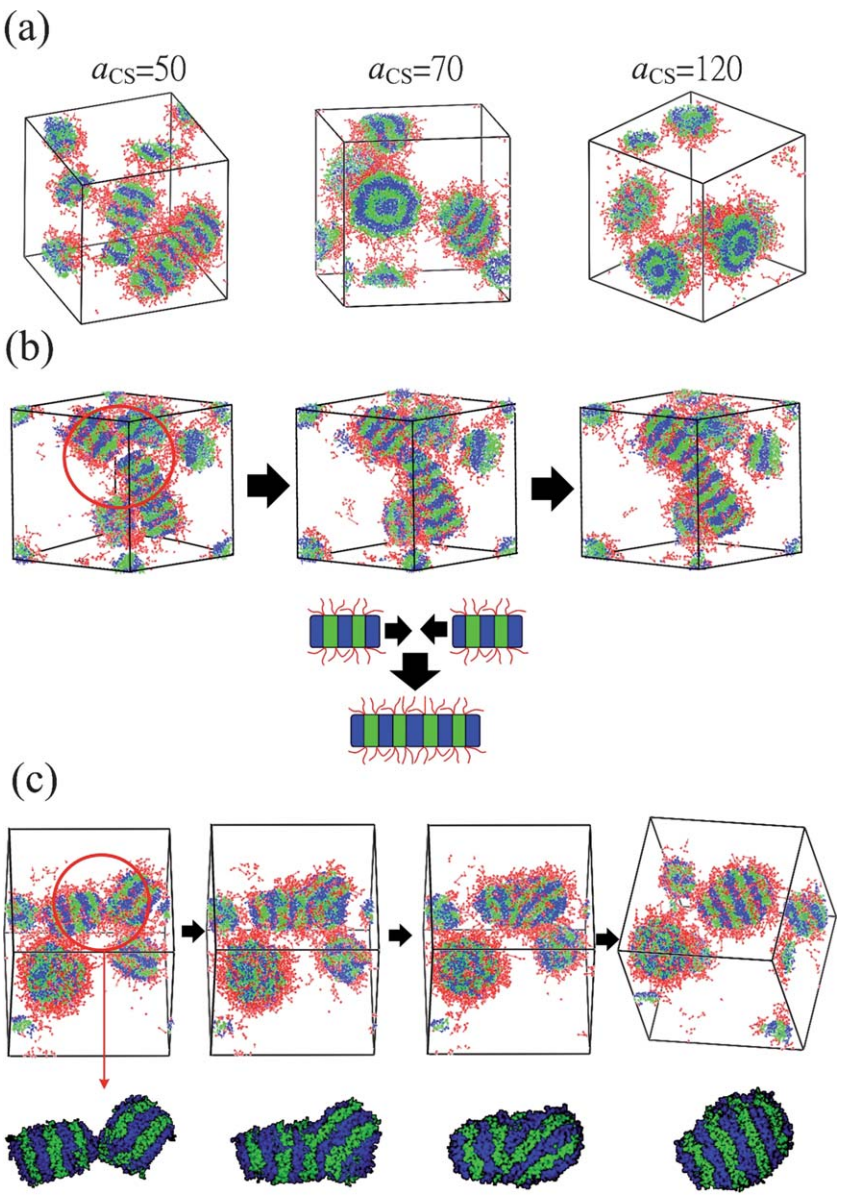

Fig. 9 (a) Morphological variation with a_{CS} at a fixed $a_{BS} = 50$. (b) Typical snapshots of micelle formation with time at $a_{BS} = 90$ and $a_{CS} = 50$. (c) Typical snapshots of micelle formation with time at $a_{BS} = 120$ and $a_{CS} = 50$. All the other parameters are the same as those in Fig. 8. The red, green, and blue colors represent A, B, and C, respectively. Solvent S is omitted here for clarity.

demonstrated in Fig. 9b and c, respectively. When $a_{BS} = 90$, we observe that these micelles are likely to approach one another more closely, and thus the B and C segmented layers can pack to form more elongated micelles as time increases. The micelle coalescence is mainly attributed to the fact that the solvophilic A block is not long enough to shield both the top and bottom C layers. When a_{BS} increases to the significantly larger value of 120, we still observe the coalescence of micelles, but the molecules seem to reorganize and form larger spherical micelles, within which the segmented layers become more disk-like. Indeed, this is not surprising since the interfacial free energy between B and S can be significantly reduced by doing so.

In Fig. 10, we display the morphology map in terms of a_{BS} and a_{CS} when f_A increases to 0.51. As discussed above, similar effects of varying the solvophobic degree of B and C on the molecular packing into the small-length-scale segregated layers are also observed here. However, based on the fact that varying the composition f_A has a great influence on the resultant overall shape of micelles, increasing f_A from 0.27 to 0.51 reveals other new micelle structures when $a_{BS} \neq a_{CS}$. In particular, when $a_{BS} > a_{CS}$, we observe the formation of B and C segmented short cylinders. When $a_{CS} > a_{BS}$, in addition to short cylinders and bowl-like micelles, within which the BC-segregated layers adopt a coaxial packing, B–C–B hamburger micelles are also possible to form. This well-segregated B–C–B packing may not provide a better shielding effect from the contacts with solvent than the coaxial packing. However, when the solvophilic A blocks become longer, they can help reduce the contacts between C and solvent, and thus enhance the well-segregated B–C–B packing path within micelles. If f_A increases to a larger value of 0.7 (Fig. 11), the formation of hamburger-like micelles becomes more prevalent, as expected. Therefore, we do not find any micelles with coaxial packing of BC layers, but only the B–C–B hamburgers in addition to the continuous B helix in the region of $a_{CS} > a_{BS}$. When the solvent dislikes B more than C ($a_{BS} > a_{CS}$), a gradual transition from B helices → C helices → C–B–C hamburgers occurs with increasing a_{BS}.

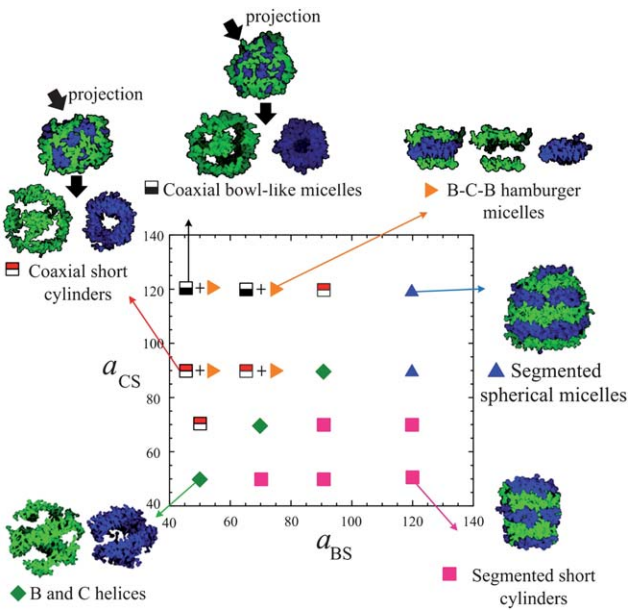

Fig. 10 Phase diagram of A_2-*star*-(B-*alt*-C) copolymer solutions in terms of a_{BS} and a_{CS} when $f_A = 0.51$, $N = 33$, $\phi = 0.13$, $a_{AB} = a_{AC} = 50$, $a_{BC} = 90$, and $a_{AS} = 25$. The same symbols represent similar micellar structures. In each representative micelle, B and C domains are shown *via* the green and blue colors, respectively, and both A and S are omitted, for clarity.

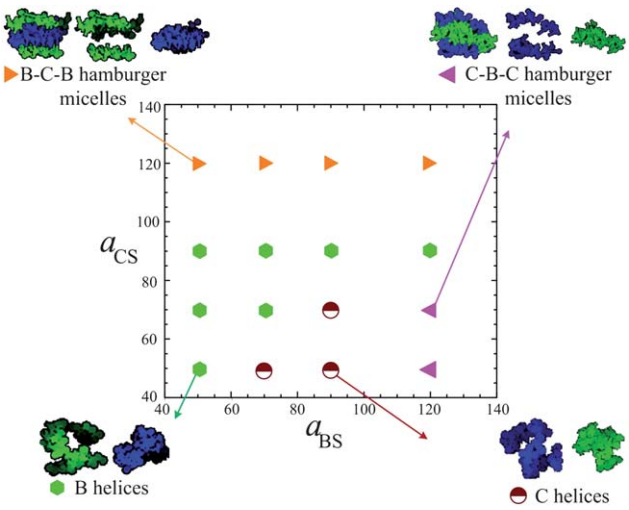

Fig. 11 Phase diagram of A_2-*star*-(B-*alt*-C) copolymer solutions in terms of a_{BS} and a_{CS} when $f_A = 0.7$, $N = 33$, $\phi = 0.13$, $a_{AB} = a_{AC} = 50$, $a_{BC} = 90$, and $a_{AS} = 25$. The same symbols represent similar micellar structures. In each representative micelle, B and C domains are shown *via* the green and blue colors, respectively, and both A and S are omitted, for clarity.

4. Conclusions

We have used dissipative particle dynamics to explore the formation of multicompartment micelles in solutions of A_2-*star*-(B-*alt*-C) polymers. The A blocks are under good solvent conditions, whereas B and C are both solvophobic, and thus can potentially form separate nanoscopic domains with the micelles. Phase maps of micelle morphology have been developed, as a function of the binary interaction parameters among A, B, and C components, and for various fractions of the A block. In addition, the effect of solvent selectivity with respect to B and C is also considered. Overall, a rich variety of multicompartment micelle morphologies are observed, including: spherical and short cylindrical micelles with disordered, concentric (coaxial) lamellar, or segmented lamellar B and C domains in the core; hamburger micelles, with one C domain sandwiched between two B layers or one B domain sandwiched between two C layers (C–B–C) in the core; segmented worm-like micelles, with alternating B and C layers along the cylinder axis; cores with helical B and C domains. The choice of core shape and internal structure can be understood in terms of the relative block volume fractions and the relative interfacial energies of the various blocks to one another, and to the solvent. The DPD method affords an efficient way to screen promising molecular architectures for the ability to self-assemble into technologically promising hierarchical structures.

Acknowledgements

This work was supported by the National Science Council of the Republic of China through grant NSC 97-2628-E-002-001-MY3, and in part by the MRSEC program of the National Science Foundation through Award DMR-0819885 (T.P.L.).

References

1 G. M. Bucknall and B. Grzybowski, *Science*, 2002, **295**, 2418.
2 O. Ikkala and G. ten Brinke, *Chem. Commun.*, 2004, 2131.
3 J.-F. Lutz and A. Laschewsky, *Macromol. Chem. Phys.*, 2005, **206**, 813.
4 T. P. Lodge, A. Rasdal, Z. Li and M. A. Hillmyer, *J. Am. Chem. Soc.*, 2005, **127**, 17608.
5 Y. Nagata, J. Masuda, A. Noro, D. Cho, A. Takano and Y. Matsushita, *Macromolecules*, 2005, **38**, 10220.
6 J. Masuda, A. Takano, Y. Nagata, A. Noro and Y. Matsushita, *Phys. Rev. Lett.*, 2006, **97**, 098301.
7 J. Masuda, A. Takano, J. Suzuki, Y. Nagata, A. Noro, K. Hayashida and Y. Matsushita, *Macromolecules*, 2007, **40**, 4023.
8 G. Fleury and F. S. Bates, *Macromolecules*, 2009, **42**, 1691.
9 G. Fleury and F. S. Bates, *Macromolecules*, 2009, **42**, 3598.
10 C. Guillermo Alfonzo, G. Fleury, K. A. Chaffin and F. S. Bates, *Macromolecules*, 2010, **43**, 5295.
11 R. Nap, I. Erukhimovich and G. ten Brinke, *Macromolecules*, 2004, **37**, 4296.
12 R. Nap, N. Sushko, I. Erukhimovich and G. ten Brinke, *Macromolecules*, 2006, **39**, 6765.
13 C. I. Huang and C. M. Chen, *ChemPhysChem*, 2007, **8**, 2588.
14 A. Subbotin, T. Klymko and G. ten Brinke, *Macromolecules*, 2007, **40**, 2915.
15 W. Li and A. C. Shi, *Macromolecules*, 2009, **42**, 811.
16 L. Wang, J. Lin and L. Zhang, *Macromolecules*, 2010, **43**, 1602.
17 M. W. Matsen and F. S. Bates, *Macromolecules*, 1996, **29**, 1091.
18 G. M. Grason and R. D. Kamien, *Macromolecules*, 2004, **37**, 7371.
19 H. Ringsdorf, P. Lehmann and R. Weberskirch, Multicompartmentation—a Concept for the Molecular Architecture of Life, in *217th ACS National Meeting*, Anaheim, CA, 1999.
20 A. Laschewsky, *Curr. Opin. Colloid Interface Sci.*, 2003, **8**, 274.
21 Z. Li, E. Kesselman, Y. Talmon, M. A. Hillmyer and T. P. Lodge, *Science*, 2004, **306**, 98.
22 J.-F. Lutz and A. Laschewsky, *Macromol. Chem. Phys.*, 2005, **206**, 813.
23 G.-E. Yu and A. Eisenberg, *Macromolecules*, 1998, **31**, 5546.
24 M. R. Talingting, P. Munk, S. E. Webber and Z. Tuzar, *Macromolecules*, 1999, **32**, 1593.
25 J.-F. Gohy, N. Willet, S. Varshney, J.-X. Zhang and R. Jérôme, *Angew. Chem., Int. Ed.*, 2001, **40**, 3214.
26 S. Kubowicz, J.-F. Baussard, J.-F. Lutz, A. F. Thünemann, H. V. Berlepsch and A. Laschewsky, *Angew. Chem., Int. Ed.*, 2005, **44**, 5262.
27 J. Hu, G. Njikang and G. Liu, *Macromolecules*, 2008, **41**, 7993.
28 X. Jiang, G. Zhang, R. Narain and S. Liu, *Langmuir*, 2009, **25**, 2046.
29 K. Skrabania, A. Laschewsky, H. V. Berlepsch and C. Bottcher, *Langmuir*, 2009, **25**, 7594.
30 K. Skrabania, H. V. Berlepsch, C. Bottcher and A. Laschewsky, *Macromolecules*, 2010, **43**, 271.
31 A. Walther, C. Barner-Kowollik and A. H. E. Müller, *Langmuir*, 2010, **26**, 12237.
32 Z. Li, M. A. Hillmyer and T. P. Lodge, *Macromolecules*, 2004, **37**, 8933.
33 Z. Li, M. A. Hillmyer and T. P. Lodge, *Langmuir*, 2006, **22**, 9409.
34 Z. Li, M. A. Hillmyer and T. P. Lodge, *Nano Lett.*, 2006, **6**, 1245.
35 Z. Li, M. A. Hillmyer and T. P. Lodge, *Macromolecules*, 2006, **39**, 765.
36 N. Saito, C. Liu, T. P. Lodge and M. A. Hillmyer, *Macromolecules*, 2008, **41**, 8815.
37 A. Walther and A. H. E. Müller, *Chem. Commun.*, 2009, 1127.
38 Z. Ge and S. Liu, *Macromol. Rapid Commun.*, 2009, **30**, 1523.
39 C. Liu, M. A. Hillmyer and T. P. Lodge, *Langmuir*, 2009, **25**, 13718.
40 K. Khanna, S. Varshney and A. Kakkar, *Macromolecules*, 2010, **43**, 5688.
41 N. Saito, C. Liu, T. P. Lodge and M. A. Hillmyer, *ACS Nano*, 2010, **4**, 1907.
42 P. J. Hoogerbrugge and J. M. V. A. Koelman, *Europhys. Lett.*, 1992, **19**, 155.
43 R. D. Groot and P. B. Warren, *J. Chem. Phys.*, 1997, **107**, 4423.
44 P. Espanol and P. B. Warren, *Europhys. Lett.*, 1995, **30**, 191.
45 M. P. Allen and D. J. Tildesley, *Computer Simulation of Liquids*, Clarendon, Oxford, 1987.
46 A. F. Jakobsen, O. G. Mouritsen and G. Besold, *J. Chem. Phys.*, 2005, **122**, 204901.
47 M. P. Allen, *J. Phys. Chem. B*, 2006, **110**, 3823.
48 U. Micka and K. Binder, *Macromol. Theory Simul.*, 1995, **4**, 419.
49 Y. Bahbot-Raviv and Z. G. Wang, *Phys. Rev. Lett.*, 2000, **85**, 3428.
50 Q. Wang, P. F. Nealey and J. J. de Pablo, *Macromolecules*, 2001, **34**, 3458.
51 R. D. Groot, T. J. Madden and D. J. Tildesley, *J. Chem. Phys.*, 1999, **110**, 9739.
52 G. H. Fredrickson and E. Helfand, *J. Chem. Phys.*, 1987, **87**, 697.
53 H. Xiang, K. Shin, T. Kim, S. I. Moon, T. J. McCarthy and T. P. Russell, *Macromolecules*, 2005, **38**, 1055.